$LaCaMgNi_9$ synthesized by mechanical alloying: Structural and electrochemical characterization

Safa Chebab[a], Mohieddine Abdellaoui[a*], Michel Latroche[b] and V. Paul-Boncour[b]

[a] *Laboratoire des matériaux Utiles, Institut National de Recherche et d'Analyses Physico-chimique, Pole technologique de Sidi Thabet, 2020 Sidi Thabet, Tunisia*
[b] *ICMPE-CMTR ; CNRS-UPEC, 2-8 rue Henri Dunant, 94320 Thiais Cedex, France*

(Received: 07 January 2016, accepted 30 January 2016)

Abstract: The performance of a nickel-metal hydride (Ni-MH) battery mainly depends on the characteristics of the negative electrode. The electrochemical characteristics of mechanically alloyed compound $LaCaMgNi_9$, including the discharge capacity and the hydrogen diffusion coefficient, were studied as function of mechanical alloying (MA) conditions. The electrochemical measurements show that the $LaCaMgNi_9$ electrode has a maximum discharge capacity of 150 mAh/g at a discharge rate of C/3. The hydrogen discharge capacity decreases dramatically when the MA exceeds 20h.

Keywords: AB_3-type alloy, mechanical alloying, electrochemical characteristics

Résumé: Les performances d'une batterie Nickel-hydrure métallique (Ni-MH) dépendent essentiellement des caractéristiques de l'électrode négative. Les caractéristiques électrochimiques du composé $LaCaMgNi_9$ obtenu par mécanosynthèse, telles que la capacité de décharge et le coefficient de diffusion de l'hydrogène, ont été étudiées en fonction des conditions de mécanosynthèse. Les caractérisations électrochimiques montrent que l'électrode formée par du $LaCaMgNi_9$ possède une capacité maximale de décharge de 150 mAh/g à un régime de C/3. La capacité de décharge maximale décroit subitement dès que la durée de mécanosynthèse dépasse 20 h.

Mots clés : Composés type AB_3, mécanosynthèse, caractérisation électrochimique.

INTRODUCTION

Hydrogen is considered as a promising sustainable energy carrier due to its high energy density and the fact that it can be produced from a variety of renewable sources including biomass and water electrolysis. In addition, hydrogen combustion does not emit green-house gases to the atmosphere which justifies its classification as a clean source of energy. For the use of hydrogen as an energy source, its safe and efficient storage is a key requirement, yet remain a challenging issue [1].

Hydrogen storage alloys have been extensively studied for many years as negative electrode materials of Ni-MH batteries [2-6]. Among the various kinds of hydrogen storage materials for Ni -MH batteries, the AB_5-type compounds display an average maximum discharge capacity of 300 mAh/g. However, none of the currently commercialized electrode alloys, including AB_5 and AB_2-types, can meet the demand of power battery owing to the limitation of their properties, such as low discharge capacity for the AB_5-type compounds and poor activation capability for the AB_2-type Laves phase electrode alloy. Therefore, one of the main challenges in this area is to find a new type of electrode materials with higher capacity and longer life cycle.

Recently , La-Mg-Ni hydrogen storage alloys, with $PuNi_3$-type structure, have been considered as promising candidates owing to the benefit of lower cost, higher discharge capacity and good electrochemical properties compared to AB_5-type alloys [7-11].

* Corresponding author, e-mail address : mohieddine.abdellaoui@yahoo.fr, Tel: +216 98 202 065

Kadir et al. [11, 12] revealed that RMg_2Ni_9 (*R*=rare earth, Ca or Y) alloys keep the $PuNi_3$-type rhombohedral structure after hydriding, and that their hydrogen storage capacity, which could reach 1.7%-1.8% (mass fraction), was significantly higher than that of the mischmetal-based AB_5-type alloys.

Chen et al. [7] have prepared by induction melting several kinds of R-Mg-Ni based alloys with $PuNi_3$-type structure. Subsequently, they found that the discharge capacity of $LaCaMgNi_9$ alloy could reach 360 mAh/g (1.87 wt;%), but the high-rate dischargeability and cyclic stability were poor.

In this work $LaCaMgNi_9$ compound was prepared by mechanical alloying (MA) in order to avoid inherent problems of the melting techniques [13]. It is now established that MA is an efficient process to synthesize a wide variety of equilibrium and non-equilibrium structures in solid state. The synthesized alloys exhibit a good compositional and microstructural homogeneity with nanometric sized particles due to the high energy impact during milling. Nanostructuring is one of the possible approaches to improve the hydrogenation properties of these materials [14, 15]. The aim of this work was to study the nanostructuring effect on the electrochemical properties of $LaCaMgNi_9$-type alloy.

EXPERIMENTAL DETAILS

Elemental La, Ca, Mg and Ni powders (with at least 99.9% purity) were mixed with the nominal composition $LaCaMgNi_9$ and charged into carbide vials under controlled atmosphere (purified argon in glove box). MA was performed with a Fritsch Pulverisette P7 planetary ball mill at rotation speed of 400 rpm with a ball to powder ratio equal to 17:1. The MA duration was varied from 4 to 30 hours and the samples were labeled Sd (S for sample and d for duration in hour).

Each powdered sample was sieved to a particle size below 40 µm for X-ray powder diffraction (XRD) analysis. XRD patterns were recorded with a (θ-2θ) Panaltytical X'Pert pro MPD diffractometer with a copper anti-cathode ($\lambda_{CuK\acute{a}}$=0.15406 nm) in a 2θ range of 10° to 100°. The XRD data were analyzed by the Rietveld method [16, 17] using FULLPROF program [18].

Working electrodes were prepared by mixing the alloy powders with black carbon and PTFE in respectively 90%, 5% and 5% weight proportions. Electrochemical measurements were performed in a conventional three electrodes open-air cell using a VMP biologic potentiostat-galvanostat. The discharge capacities of the electrodes were determined at room temperature by galvanostatically charge-discharge at respectively C/3 and C/6 rates. The $Ni(OH)_2$/NiOOH and Hg/HgO electrodes were used as the counter and the reference electrodes respectively. Cyclic voltammetry was performed for different scan rates in the -0.5 to -1.1 V potential range. The chronoamperometry was applied after 30 cycles of charge-discharge. This method consists in fully charging and discharging the electrode at constant potential (-0.6 V vs Hg/HgO).

EXPERIMENTAL RESULTS AND DISCUSSION

1. Structural properties of the alloys

Starting from elemental La, Ca, Mg and Ni metals, MA leads to the formation of a mixture of nanocrystalline AB_3-type phase with $PuNi_3$-type structure (S.G: *R-3m*) and $LaNi_5$ phase since 10 h of MA.

Fig. 1 gives the XRD patterns of the samples alloyed for different times. In the XRD pattern of the un-milled sample (S0), all the diffraction lines of the starting elements are present. The diffraction peaks of nickel are the most intense, while those of the other elements are barely detectable. This fact

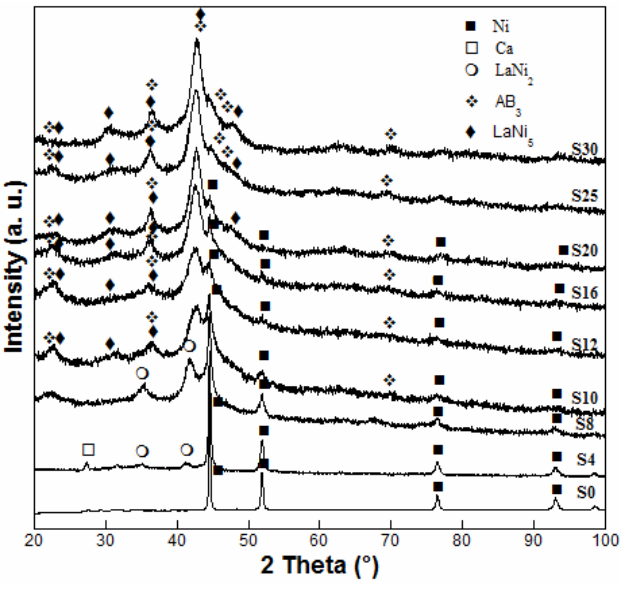

figure 1: Evolution of the XRD patterns of samples for increasing MA duration (4 to 30 hours).

Table I: Phase structural properties and maximum discharge capacities of the samples synthesized by MA at various milling time

Sample St	Phase	Space group	Phase abundance (wt%)	C_{max} (mAh/g of active material)	C_{10} (mAh/g of active material)	Loss of charge after 10 cycles (%)
S10	AB_3 $LaNi_5$ Ni	*R-3m* *P6/mmm* *Fm-3m*	42.7 (1.6) 40.1 (1.4) 17.2 (0.7)	130.4	107,8	17.3
S12	AB_3 $LaNi_5$ Ni	*R-3m* *P6/mmm* *Fm-3m*	48.4 (1.5) 40.9 (1.3) 10.7 (0. 6)	124.9	120.2	3.51
S16	AB_3 $LaNi_5$ Ni	*R-3m* *P6/mmm* *Fm-3m*	49.8 (1.3) 45.6 (1.2) 4.6 (0.5)	141.3	122.1	12.7
S20	AB_3 $LaNi_5$ Ni	*R-3m* *P6/mmm* *Fm-3m*	52.2 (1.4) 43.1 (1.2) 4.7 (0.5)	156.1	117.1	24.2
S25	AB_3 $LaNi_5$	*R-3m* *P6/mmm*	53.5 (1.7) 46.5 (1.3)	138.2	121.5	11.8
S30	AB_3 $LaNi_5$	*R-3m* *P6/mmm*	67 (1.8) 33 (1.2)	121.6	95.4	21.2

is mainly related to the low contents of Ca, Mg and La, 5.47, 3.32 and 18.9wt% respectively, in comparison with the Ni one (72.21 wt %).

X-ray diffraction patterns of the mechanically alloyed powders reveal a modification of the microstructure of the powders during MA process. With increasing MA duration, the originally sharp diffraction lines of the powders show a remarkable line broadening and an intensity reduction compared to the S0 sample. It indicates a decrease of the crystallite size and a presence of lattice microstrains within the particles. Furthermore, MA for longer time results in the partial amorphization of the alloy. In fact, the increase of MA duration induces more strains and increases the defect concentration in the crystalline structure of elemental powders, leading to a partial amorphization of the sample.

As observed, Ni particles remains present up to 20 hours of MA, while other elements are no more observed after the first hours of milling. Depending on MA duration, the formation of an AB_3-type phase with a $PuNi_3$-type structure occurred in coexistence with $LaNi_5$ (S.G: *P6/mmm*). The $LaNi_2$-type phase appears as an intermediate phase for an MA duration ranging from 4 to 8h and disappears hereafter.

The composition and lattice parameters of the phases were calculated by the Rietveld method and are listed in Table 1. As the MA duration increases, the abundance of the $LaCaMgNi_9$ AB_3-type phase increases from about 43 wt% to 63 wt% whereas that of $LaNi_5$ increases first from 40 wt% to 47 wt% then decreases to 36 wt %.

The SEM micrograph presented in figure 2 shows the morphology of the S30 sample. The powder is composed of large agglomerates of more than 5µm in size. These agglomerates are made of several smaller (0.1- 1µm) deformed particles welded together.

2. Electrochemical characterizations

2. 1. Activation and charge-discharge cycle stability of the alloys

The variation of the measured discharge capacities of the mechanically alloyed samples as a function of the charge-discharge cycle number is shown in figure 3. For all samples, the maximum discharge capacity was reached at the first cycle, and then slightly decreases for the next cycles to remain stable at a higher cycle number. This decrease can be attributed to the corrosion of the active phase in the electrolyte during the reaction.

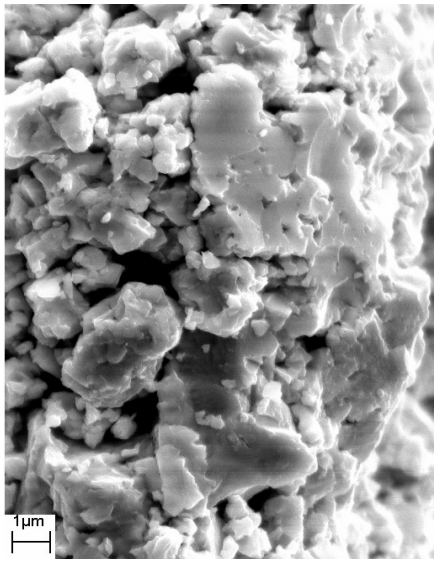

figure 2: SEM micrography showing the morphology of the S30 sample.

As the alloy contains some phases that do not absorb hydrogen, the discharge capacity of the active material ($C_{activematerial}$, Table 1) was calculated based on the measured discharge capacity of the hole material (Fig. 3) and the contributions of the hydrogen absorbing phases only (AB_3-type and $LaNi_5$ phases), as:

$$C_{activematerial} = C_{measured}/(x + y) \quad (1)$$

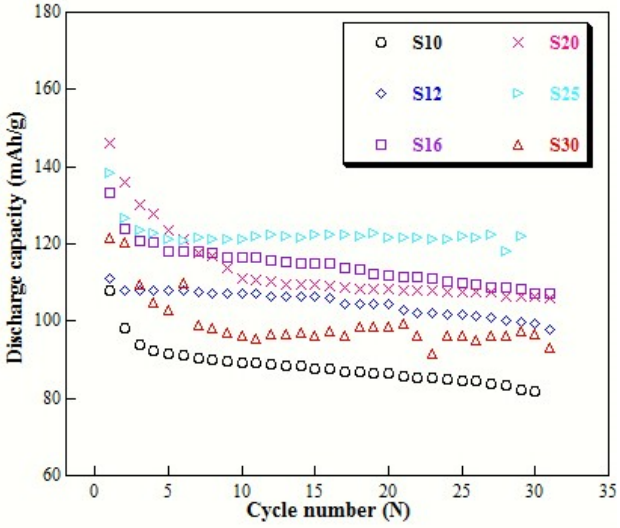

figure 3: Variation of the discharge capacity vs cycle number of S10 to S30 samples

Where:
$C_{measured}$ is the measured discharge capacity (of the whole material), x and y are respectively the $LaNi_5$ and the AB_3-type phase contents.
The effect of the MA duration on the discharge capacities of the active material, at first and 10^{th} charging-discharging cycle are shown in figure 4. It shows that the discharge capacity increases up to 20 hours of milling to reach about 156 mAh/g. Above 20h, the discharge capacity decreases with MA duration reaching values comparable to the ones obtained at lower milling duration.
The storage capacity reduction with the MA duration is attributed to a creation of defects in the material during the synthesis process. During MA, the powder particles which are trapped between the colliding balls are subjected to compressive impact forces. Thus, they are deformed, fractured and cold -welded leading to defects in the system and to a reduction in the average particle size [19].
As mentioned before, the discharge capacity of $LaCaMgNi_9$ alloy could reach 360 mAh/g [7] while the maximum discharge capacity obtained in this work is 156 mAh/g of active material (146.2 mAh/g for sample S20) after 20 h of MA. In addition, it is importante to know the contribution of each phase to the total discharge capacity, as samples are formed by two hydrogen absorbing phases ($LaNi_5$ and AB_3-type phase). For a polyphasic alloy, the total measured electrochemical discharge capacity would be equal to the sum of the contributions of all phases as:

$$C_{measured}(\text{mAh/g of alloy}) = \sum_i x_i C_{\varphi_i} \quad (2)$$

Where x_i and C_{φ_i} are respectively the weight content and the electrochemical discharge capacity of the phase φ_i. As mentioned above only $LaNi_5$ and AB_3-type phase are the hydrogen absorbing phases, in fact, the total measured electrochemical discharge capacity can be expressed as:

$$C_{measured}(\text{mAh/g of alloy}) = x * C_{LaNi_5} + y * C_{AB_3-typephase} \quad (3)$$

where:
x and y are respectively $LaNi_5$ and AB_3-type phase weight contents and C_{LaNi_5} and C_{AB_3} are respectively the discharge capacity of $LaNi_5$ and AB_3-type phase.

In order to determine the maximum discharge capacity of the obtained AB_3-type phase, we measured the discharge capacity of $LaNi_5$ synthesized in the same energetic condition of the AB_3-type . The obtained value is 180 mAh/g. The discharge capacity of the AB_3-type phase is expressed as below:

$$C_{AB_3-typephase} = [C_{measured} - (x * C_{LaNi_5})]/y \quad (4)$$

Using expression (4), the maximum discharge capacity of the formed AB_3-type phase is about 135 mAh/g. Thus, as the discharge capacity of the $LaNi_5$ is higher than the one of AB_3-type phase, the decrease of the total measured electrochemical discharge capacity (the electrochemical discharge capacity) of the active material, beyond 20 h of MA (figure 4), is attributed to the decrease of the $LaNi_5$ weight content.

The activation capability is a very important performance for the practical use of Ni-MH battery. It is usually characterized by the number of charge-discharge cycles required to reach the greatest discharge capacity at constant current density. The smaller cycles number, the better activation performance. The examination of the variation of discharge capacity as function of the cycle number (figure 3) reveals that the alloys possesses good activation performances, attaining their maximum discharge capacities at the first cycle.

Compared to the electrochemical discharge capacity, the PCT curve, shown in fig.5, indicates a hydrogen absorption capacity, at low pressure, of about 5 H/f.u [13]. This value is representative of the whole sample and involves the two hydrogen absorbing phase $LaNi_5$ and $LaCaMgNi_9$ type phases.

2. 2. Determination of kinetic parameters of the hydrogen absorption reaction

a) Cyclic voltametry

Figure 6 shows the cyclic voltammograms for the S30 sample. The working electrode potential was scanned from -1.1 to -0.5 V versus Hg/HgO (1 $mol.L^{-1}$ KOH solution) with scan rates of 10, 20, 30, 40 and 50µV/s. The anodic and cathodic peaks reflect the information related to the discharge and charge processes [20]. The observed anodic peak is attributed to the oxidation of the desorbed hydrogen atoms at the surface while the cathodic peak is attributed to the reduction of hydrogen atoms absorbed by the alloy in the interstitial sites. As seen in figure 6, the anodic peak current increases and its potential shifts towards positive direction with increasing scan rate.

Figure 7-a gives the variation of the anodic peak potential of the S30 alloy as function of log (v). This relation is linear. In this case, the anodic peak potential can be written as follows:

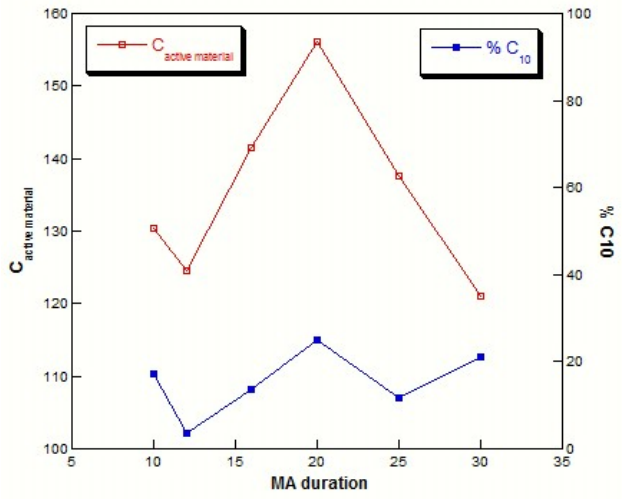

figure 4: Effect of MA duration on the dischage capacities of the active material at the first cycle and the loss of discharge capacity at the 10th charging-discharging cycle.

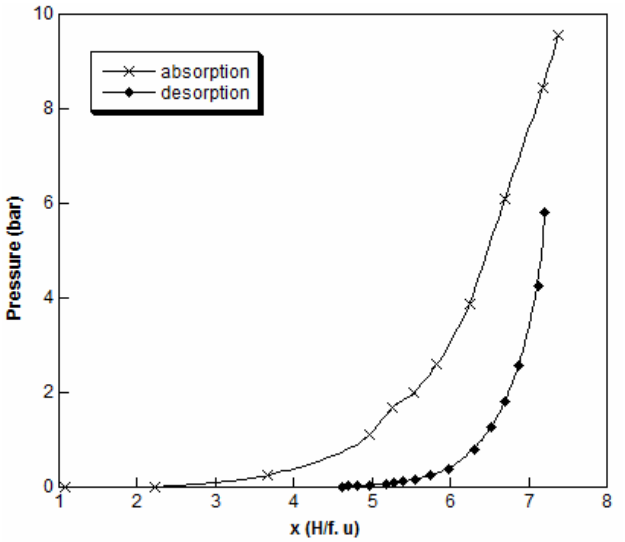

Fig. 5 : PCT curve of the S30 sample measured at 25 °C [13].

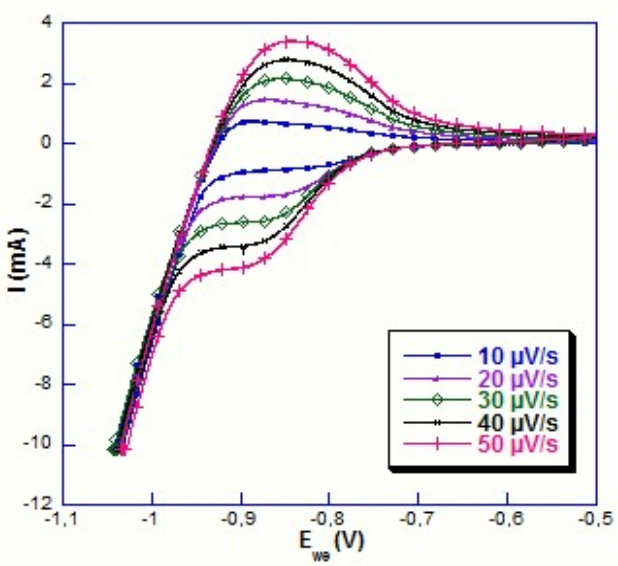

figure 6: Cyclic voltammograms of S30 sample at potential scan rate: 10, 20, 30, 40 and 50 µV/s.

$$\frac{dE_{ap}}{d\log(v)} = \frac{2.3RT}{2\alpha nF} \qquad (5)$$

With *R*: gas constant, *F*: Faraday constant and *T* as Temperature.

This equation allows the determination of the charge transfer coefficient α (Table 2). This parameter indicates the alloy ability to charge and discharge. As the á value ranges from 0.3 to 0.7, it can be approximated to be close to 0.5 [21], which means that the charge and discharge are reversible and the system has the same tendency for the charge as for the discharge process.

Fig. 7-b shows that the variation of the anodic current peak with the square root of the scan rate $v^{1/2}$ is linear. So, for semi infinite diffusion and irreversible transfer, the current of the anodic oxidation peak is expressed as follows:

$$I_{pic} = 2{,}99.10^5.C_o.\alpha^{1/2}.S.D^{1/2}.\sqrt{v}$$

From the slope of this curve, as we know 'α' values, we can determine the average hydrogen diffusion coefficient in the material if the electrode surface is known, and vice versa. When using the Latex technology for the electrode preparation, and its value was slightly different from the geometrical value due to its porous surface. So, the hydrogen diffusion coefficient will be determined with another technique as chronoamperometry, for example.

b) Chronoamperometry

Fig. 8 shows the current responses expressed in log (i) versus time for the synthesized alloys at 298 K. The semi logarithmic curves of anode current density versus time can be divided in two time region. In the first one the current decreases rapidly due to a consumption of hydrogen at the surface, while in the second time region the current

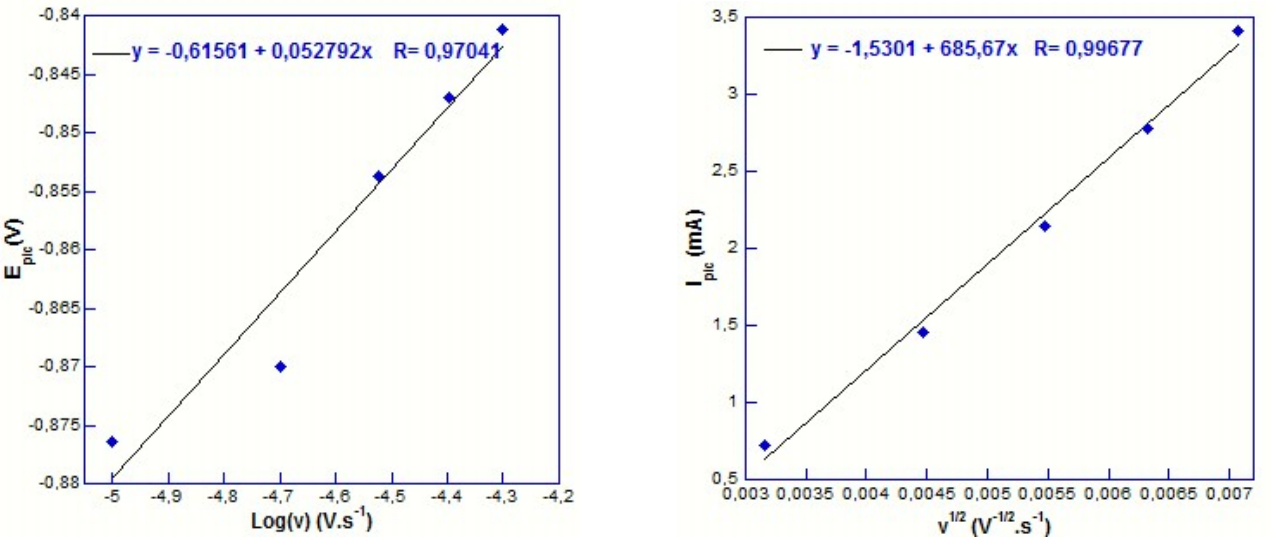

a) **b)**

figure 7: a) Variation of the anodic peak potential as function of log (v) and b) Variation of the anodic peak current as function of square (v) of cyclic voltammograms of S30 sample.

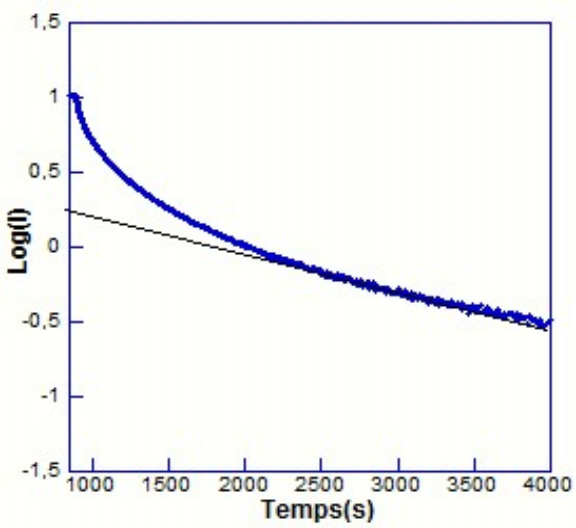

figure 8: Semilogarithmic plots of anodic current-time responses of the S30 sample.

decreases slowly in a linear way. In this case, hydrogen is supplied from the bulk alloy proportionally to the concentration gradient of hydrogen. The current is controlled by the diffusion rate of hydrogen atoms [22] with time [23, 24].

As all samples are multi-phases, the calculated coefficient of hydrogen diffusion is an average value describing the hydrogen diffusion in the whole sample not in a specific phase. From the slope of the linear region in fig. 8, it is possible to estimate the average coefficient of hydrogen diffusion value using the following formula, which is valid at a large time [25]:

$$\log(i) = \log(\frac{6FD}{da^2})(C_0 - C_s) - (\frac{\pi^2 D}{2.303a^2})t \quad (6)$$

$$D = -\frac{2.303a^2}{\pi^2}\frac{d\log(i)}{dt} \quad (7)$$

Where *i, D, d, a, C_0, Cs* and *t* are respectively : the diffusion current ($A.g^{-1}$), the diffusion coefficient of hydrogen ($cm^2.s^{-1}$), the density of hydrogen storage, the alloy particle radius (cm), the initial hydrogen concentration in the bulk of alloy ($mol.cm^{-3}$),and the hydrogen concentration on the surface of the alloy particle radius respectively. Assuming that the average particle radius is *a*=5µm (SEM micrograph figure2), *D* can be calculated according to equation (3) and the calculated values are listed in Table 2. As we can notice, the diffusion coefficient of hydrogen *D* shows the same behaviour than the discharge capacity as a function of MA duration. Its value increases up to 20 h of MA and decreases for larger time.

Table II: Charge transfer coefficient 'á' and hydrogen diffusion coefficient "D" of the S10 to S30 samples.

Sample	Charge transfer coefficient 'á'	D($cm^2.s^{-1}$)
S10	0.23	$4.9.10^{-10}$
S12	0.49	$5.1.10^{-10}$
S16	0.50	$6.3.10^{-10}$
S20	0.56	$6.8.10^{-10}$
S25	0.69	$6.2.10^{-10}$
S30	0.24	$5.9.10^{-10}$

CONCLUSION

A nanostructured $PuNi_3$-type alloy has been synthesized by mechanical alloying of a stoichiometric mixture of La, Ca, Mg and Ni elements after different milling duration. The electrochemical properties of the milled samples have been investigated by electrochemical methods: Chronopotentiometry, cyclic voltammetry and chronoamperometry. The following conclusions can be drawn:

- All samples exhibit limited discharge capacity with a maximum of about 156 mAh/g after 20h of MA. Further, the discharge capacity decreases with increasing MA duration. This is attributed to the increase of lattice defects and the decrease of particle size.
- The values of the charge transfer coefficient range from 0.3 to 0.7 for samples mechanically alloyed between 12h and 25h which indicate a good reversibility of the electrochemical reaction. For the sample milled for 10h and 30h, the á value are respectively 0.232 et 0.242.

ACKNOWLEDGEMENTS: The financial support was guaranteed by the CMCU project (CMCU PHC Utique N°10G1208).

REFERENCES

[1] S. H. Barghi, T. T. Tsotsis, *Int. J. Hydrogen Energy* **2013**; 39: 1390-97.

[2] Z. Rogulski, J. Diubak, M. Karwowska, E. Pytlik, *J. Power Sources* **2010**; 195:7517-23.
[3] S. Li, M. Zhao, L. Wang, Y. Liu, Y. Wang, *Mater. Sci. Eng. B* **2008**; 150: 168-74.
[4] D. Mu, Y. Hatano, T. Abe, K. Watannabe, *J. alloys Compd.* **2002**; 334: 232-7.
[5] K .Young, J. Nei, B. Huang, M. A. Fetcenko, *Int. J. Hydrogen Energy* **2011**; 36: 11146-54.
[6] H. Miyamura, T. Sakai, N. Kuriyama, K. Oguro, A. Kato. *Electrochem Soc. Proc*. **1992**; 92-5: 179-98.
[7] J. Chen, N. Kuriyama, H. T. Takeshita, H. Tanaka, T. Sakai, *Electrochem Solid State Letter* **2000**; 3 (6): 249-52.
[8] H. G. Pan, Y. F. Liu, M. X. Cao, Y. F. Zhv, Y. Q. Lei, Q. D. Wang, *J. Alloys Compd*. **2003**; 351:228-34.
[9] B. Liao, Y. Q. Li, L. X. Chen, G. L. Lu, H. G. Pan, *J. Alloys Compd*. **2004**; 376: 186-95.
[10] H. G. Pan, Y. F. Liu, M. X. Gao, Y. Q. Lei, Q. D. Wang, J. Electrochem Soc. 2005; 152(2): A326-32.
[11] K. Kadir, T. Sakai , I. Uehara, *J. Alloys Compd*. **1999**; 287:264-70.
[12] K. Kadir, T. Sakai , I. Uehara, *J. Alloys Compd*. **2000**; 302:112-117.
[13] S. Chebab, M. Abdellaoui, M. Latroche, V. Paul-Boncour, *Mater Renew Sustain Energy* (**2015**) 4:13
[14] B. Joseph, A. Iadecola, B. Schiavo, A. Cognigni, L. Olivi, *J. Solid State Chem*. **2010**; 183 1550.
[15] B. Joseph , B. Schiavo, *J. Alloys Compd*. **2009**; 480: 912.
[16] H. M. Rietveld. *Acta cristallgr*. **1967**; 22:151.
[17] H. M. Rietveld, *J. Appl. Cryst*. **1969**; 2: 65.
[18] J. Rodriguez-Carvajal, *J. Phys*. **1993**; 192 B: 55.
[19] Y. Wu, W. Hana, S. X. Zhou, M. V. Lototsky, J. K. Solberg, V. A. Yartys, *J. Alloys Compd*. **2008**; 466: 176.
[20] Z. Tan, Y. Yang, Y. Li, H. Shao, *J. Alloys Compd*. **2008**; 453:79-86.
[21] A. J. Bard, L. R. Fulkner, *Electrochimie: Principe, methodes et applications, Masson, Paris*, **1998**.
[22] K. Giza, *Intermetallics* 34; **2013**:128-131.
[23] G. Zheng, B. N. Popov, R. E. White, *J. Electrochem. Soc*. 142; **1995**:2695.
[24] H. Pan, N. Chen, M. Gao, *J. Alloys Compd*. 397; **2005**: 306.